Commun. Theor. Phys. **74** (2022) 015602 (9pp) https://doi.org/10.1088/1572-9494/ac3ed3

Local stability analysis of a low-dissipation cyclic refrigerator*

Kai Li[1], Jie Lin[1] and Jian-Hui Wang[1,2]

[1] Department of Physics, Nanchang University, Nanchang 330031, China
[2] State Key Laboratory of Surface Physics and Department of Physics, Fudan University, Shanghai 200433, China

E-mail: wangjianhui@ncu.edu.cn

Received 6 October 2021, revised 30 November 2021
Accepted for publication 1 December 2021
Published 13 January 2022

Abstract

We study the local stability near the maximum figure of merit for the low-dissipation cyclic refrigerator, where the irreversible dissipation occurs not only in the thermal contacts but also the adiabatic strokes. We find that the bounds of the coefficient of performance at a maximum figure of merit or maximum cooling rate in the presence of internal dissipation are identical to those in the corresponding absence of internal dissipation. Using two different scenarios, we prove the existence of a single stable steady state for the refrigerator, and clarify the role of internal dissipation on the stability of the thermodynamic steady state, showing that the speed of system evolution to the steady state decreases due to internal dissipation.

Keywords: local stability, system dynamics, low dissipation, cyclic refrigerator

(Some figures may appear in colour only in the online journal)

1. Introduction

The optimal analysis on finite-time performance of thermal machines that include heat engines and refrigerators has attracted much interest [1–24], beginning with the seminar work [1]. Among these, the low-dissipation model [12–25] in which the thermal-contact process is not quasi-static but close to the reversible limit was usually adopted, with the advantage that neither phenomenological heat-transfer laws nor quantum master equations are used. Under the low-dissipation assumption, the irreversible entropy production along a thermal-contact process is inversely proportional to the long-time duration t. Such a $1/t-$ scaling entropy production was theoretically proved in classical [26, 27] and quantum systems [28, 29], and it was also validated in recent experiments [30, 31] based on different platforms. A quite interesting topic is making a comparison between the low-dissipation model and the irreversible machines based on assumptions on the heat fluxes and considerations on the degree of irreversibility, as well as some specific models for quantum systems, showing that there is equivalence between them within certain optimal operation regime [24, 32].

When the machine proceeds in finite time, the irreversibility occurs not only along a thermal-contact process but also during a thermodynamic adiabatic process [3, 15, 33–36]. The irreversible phenomenon in the latter case is usually associated with the internal friction that accounts for the irreversible entropy production. Such friction occurring in classical [3] or quantum [34, 35] systems is related to energy dissipation owing to the timescale disparity between internal dynamics and finite-time evolution [35]. The irreversible entropy generation induced by the internal dissipation was recently proved to satisfy the $1/t^2-$ scaling form along the nonadiabatic process with time duration t [37, 38], though its exact evaluation depends on the system under consideration [34, 35]. The influence of the internal dissipation on the finite-time performance was intensively investigated for heat engines or refrigerators ranging from macroscale [15] to microscale [36–38].

While for a heat engine the optimization objective was usually power output and Omega function, for refrigerators a series of optimization criteria [15, 17] were proposed, such as per-unit-time coefficient of performance $\varepsilon/t_{\rm cyc}$, Ω optimization criterion, and figure of merit $\chi=\varepsilon Q_c/t_{\rm cyc}$, where $t_{\rm cyc}$

* Project supported by the National Natural Science Foundation of China (Grant No. 11875034) and the Opening Project of Shanghai Key Laboratory of Artificial Microstructure Material and Technology.

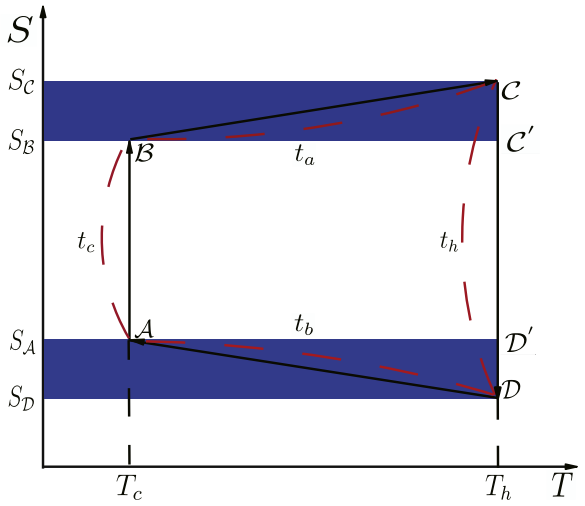

Figure 1. Schematic diagram of an irreversible refrigeration cycle in the plane of temperature T and entropy S. Here $S_z (z = \mathcal{A}, \mathcal{B}, \mathcal{C}, \text{and } \mathcal{D})$ are entropies at four instants ($\mathcal{A}$, $\mathcal{B}$, $\mathcal{C}$, $\mathcal{D}$). $t_{c,h}$ are the time durations spent on the two thermal contacts, while $t_{a,b}$ are the times taken for the two adiabatic strokes. The blue areas defined by the rectangles $\mathcal{C}$, $\mathcal{C}'$, $S_{\mathcal{B}}$, $S_{\mathcal{C}}$ and $\mathcal{D}$, $\mathcal{D}'$, $S_{\mathcal{A}}$, $S_{\mathcal{D}}$ represent the dissipated work owing to internal dissipation in the two adiabatic strokes.

is the total cycle period and $\varepsilon = -Q_c/(Q_h + Q_c)$, with $Q_c(Q_h)$ being the heat absorbed from the cold (hot) reservoir. The analysis of dynamical behavior provides a suitable way to understand the stability near the steady state which, for heat engines, corresponds to maximum power or maximum Omega function [39–42]. Since in low-dissipation models a general time-dependent formulation on irreversible entropy production are given, the stability dynamics around the stable point were proposed by analyzing the time evolution [39–42] instead of particularities in the heat exchange mechanism [43–45]. Until now, a unified description of local stability for an irreversible refrigerator, where the internal dissipation exists due to a finite-time operation, is still unavailable.

In the present paper, we study the stability properties of a finite-time refrigerator where irreversibility occurs not only from thermal contacts but also from thermodynamic adiabatic strokes. The coefficient of performance is determined by optimizing χ figure of merit and the cooling rate with respect to the time durations along the four processes. The analytical expression for the optimal coefficient of performance is obtained, showing that the internal dissipation has no influence on the upper and lower bounds of the optimal coefficient of performance under maximum cooling rate or maximum figure of merit. We clarify the role that the dissipation plays along the four strokes in the stability of the refrigerator under maximal χ figure of merit. Finally, we study the relation between internal dissipation and system relaxation speed as well as the cycle period.

2. Model

We consider a refrigeration cycle consisting of two heat transfer processes ($\mathcal{A} \to \mathcal{B}$ and $\mathcal{C} \to \mathcal{D}$) and two thermodynamic adiabatic branches ($\mathcal{B} \to \mathcal{C}$ and $\mathcal{D} \to \mathcal{A}$), as sketched in figure 1, where the time durations of the four processes are indicated by t_c, t_a, t_h, and t_b, respectively. While in the cooling or heating stroke the working substance is in contact with a cold and a hot heat bath of constant temperatures T_c and T_h, respectively, during an adiabatic branch the working substance is isolated from either the hot or cold reservoir. In the branch $\mathcal{B} \to \mathcal{C}$ ($\mathcal{D} \to \mathcal{A}$) work should be done to overcome the inner friction which results in heat, causing the entropy to increase from $S_{\mathcal{B}}(=S_{\mathcal{C}'})$ to $S_{\mathcal{C}}$ [$S_{\mathcal{D}}$ to $S_{\mathcal{A}}(=S_{\mathcal{D}'})$], irrespective of the system is expanded or compressed. The entropy variations along the cold and hot thermal contacts can be expressed as $\Delta S_c = S_{\mathcal{B}} - S_{\mathcal{A}}$, and $\Delta S_h = S_{\mathcal{D}} - S_{\mathcal{C}}$, respectively. Notably, $\Delta S_c \leftarrow \Delta S_h$ in the presence of internal friction, and $\Delta S_c = -\Delta S_h$ when friction is absent. For the engine model under consideration, the time durations $t_i (i = a, b, c, h)$ along these four irreversible processes are finite and therefore the total cycle period $t_{\text{cyc}} = t_a + t_b + t_c + t_h$ should be finite.

Let Q_c (Q_h) be a certain amount of heat along the cooling (heating) stroke; the variation of entropy can be given by

$$\Delta S_c = \frac{Q_c}{T_c} + \Delta S_c^{\text{ir}}, \tag{1}$$

or

$$\Delta S_h = \frac{Q_h}{T_h} + \Delta S_h^{\text{ir}}, \tag{2}$$

where $\Delta S_{c,h}^{\text{ir}}$ denotes the irreversible entropy production due to finite-time operation along the cooling or heating stroke, $Q_c(Q_h)$ being the heat absorbed from the cold (hot) reservoir. Unlike in the quasi-static, adiabatic process where the entropy is kept constant, along the finite-time adiabatic process the entropy increases due to the internal dissipation. Such irreversible entropy production can be determined according to $\Delta S_a^{\text{ir}} = S_{\mathcal{A}} - S_{\mathcal{D}}$ for adiabatic expansion $\mathcal{D} \to A$ and $\Delta S_b^{\text{ir}} = S_{\mathcal{C}} - S_{\mathcal{B}}$ for adiabatic compression $\mathcal{B} \to \mathcal{C}$. Since the variation of the system entropy is zero after a single cycle, we have $\Delta S + \Delta S_h + \Delta S_a^{\text{ir}} + \Delta S_b^{\text{ir}} = 0$, or

$$-\Delta S_h = \Delta S + \Delta S_a^{\text{ir}} + \Delta S_b^{\text{ir}}, \tag{3}$$

where $\Delta S \equiv \Delta S_c$ has been used. When the internal dissipation occurs along the adiabatic process due to finite-time duration, the entropy change ΔS_h during the heating process is dependent on the protocols of the two adiabatic strokes. This is quite different from entropy variation $\Delta S_c = \Delta S$ that is determined only by the initial and final states of the cooling stroke and taken as a state variable.

We now assume that the irreversible entropy production along the hot or cold thermal-contact branch is inversely proportional to the time duration for completing this stroke, quantifying irreversible entropy production as $\Delta S_{c,h}^{\text{ir}} = \Sigma_{c,h}/t_{c,h} + O(1/t_{c,h}^2)$ [13, 15, 26–31], where $\Sigma_{c,h}$ are the dissipation coefficients along the hot and cold thermal contacts, respectively. Here the higher order terms are considered negligible due to the large time durations. On the other hand, the irreversible entropy generation during a thermodynamic adiabatic process with time duration $t_{a,b}$ satisfies the $1/t_{a,b}^2$–scaling form, namely, $\Delta S_{a,b}^{\text{ir}} = \Sigma_{a,b}/t_{a,b}^2$ [37, 38]. These coefficients Σ_i ($i = c, h, a, b$) only depend on the internal dynamics of the working system, and thus they can be

considered as constants for a given machine model. Notably, the entropy generation $\Delta S^{\rm ir}_{a,b}$ depends only on the detailed protocols along during the adiabatic process, since it is a function of time durations $t_{a,b}$ only. The time spent on a thermal contact or an adiabatic branch is denoted by t_i, and thus the total cycle period is given by $t_{\rm cyc} = t_a + t_b + t_c + t_h$. Using equations (1), (2) and (3), we then arrive at

$$Q_c = T_c\Delta S\left(1 - \frac{\Sigma_c}{\Delta S t_c}\right), \tag{4}$$

$$Q_h = -T_h\Delta S\left(1 + \frac{\Sigma_a}{\Delta S t_a^2} + \frac{\Sigma_b}{\Delta S t_b^2} + \frac{\Sigma_h}{\Delta S t_h}\right). \tag{5}$$

For each cycle, the total irreversible entropy production exclusively comes from the two heat reservoirs, namely, $\sigma = -(Q_h/T_h + Q_c/T_c)$, leading to

$$\sigma = \frac{\Sigma_a}{t_a^2} + \frac{\Sigma_b}{t_b^2} + \frac{\Sigma_c}{t_c} + \frac{\Sigma_h}{t_h}. \tag{6}$$

With consideration of equations (1) and (2), the main performance parameters, which includes the cooling rate ($R = Q_c/t$), the coefficient of performance [$\varepsilon = -Q_c/(Q_h + Q_c)$], and the figure of merit ($\chi = \varepsilon R$), can be obtained:

$$R = T_c\Delta S\left(1 - \frac{\Sigma_c}{\Delta S t_c}\right)t_{\rm cyc}^{-1}, \tag{7}$$

$$\varepsilon = \frac{T_c\Delta S\left(1 - \frac{\Sigma_c}{\Delta S t_c}\right)}{T_h\Delta S\left(1 + \frac{\Sigma_a}{\Delta S t_a^2} + \frac{\Sigma_b}{\Delta S t_b^2} + \frac{\Sigma_h}{\Delta S t_h}\right) - T_c\Delta S\left(1 - \frac{\Sigma_c}{\Delta S t_c}\right)}, \tag{8}$$

$$\chi = \frac{\left[T_c\Delta S\left(1 - \frac{\Sigma_c}{\Delta S t_c}\right)\right]^2}{\left[T_h\Delta S\left(1 + \frac{\Sigma_a}{\Delta S t_a^2} + \frac{\Sigma_b}{\Delta S t_b^2} + \frac{\Sigma_h}{\Delta S t_h}\right) - T_c\Delta S\left(1 - \frac{\Sigma_c}{\Delta S t_c}\right)\right]t_{\rm cyc}}. \tag{9}$$

The coefficient of performance reaches the Carnot value, $\varepsilon_C = T_c/(T_h - T_c)$, but the cooling rate R vanishes, if and only if the cycle period $t_{\rm cyc}$ is infinitely long and the cycle is reversible.

3. Coefficient of performance under maximum cooling power and maximum figure of merit

We define the following dimensionless or scaled variables, which are

$$M_a = \frac{\Sigma_a}{\Sigma_h}, M_b = \frac{\Sigma_b}{\Sigma_h}, M_c = \frac{\Sigma_c}{\Sigma_h}, \tilde{t}_a = \frac{\Delta S}{\Sigma_h}t_a,$$
$$\tilde{t}_b = \frac{\Delta S}{\Sigma_h}t_b, \tilde{t}_c = \frac{\Delta S}{\Sigma_h}t_c, \tilde{t}_h = \frac{\Delta S}{\Sigma_h}t_h. \tag{10}$$

With these, the dimensionless heats [$\tilde{Q}_c = Q_c/(T_h\Delta S)$ and $\tilde{Q}_h = Q_h/(T_h\Delta S)$] exchanged along the two thermal contacts can be obtained from equations (4) and (5),

$$\tilde{Q}_c = \tau\left(1 - \frac{M_c}{\tilde{t}_c}\right), \tag{11}$$

$$\tilde{Q}_h = -\left(1 + \frac{M_a}{\tilde{t}_a^2} + \frac{M_b}{\tilde{t}_b^2} + \frac{1}{\tilde{t}_h}\right), \tag{12}$$

with $\tau = T_c/T_h$. It follows that, the normalized forms of equations (7), (8), and (9) are

$$\tilde{R} = \left(1 - \frac{M_c}{\tilde{t}_c}\right)\frac{\tau}{\tilde{t}_{\rm cyc}}. \tag{13}$$

$$\tilde{\varepsilon} = \frac{\tau(1 - \frac{M_c}{\tilde{t}_c})}{\left(1 + \frac{M_a}{\tilde{t}_a^2} + \frac{M_b}{\tilde{t}_b^2} + \frac{1}{\tilde{t}_h}\right) - \tau\left(1 - \frac{M_c}{\tilde{t}_c}\right)}, \tag{14}$$

$$\tilde{\chi} = \frac{\left(\tau - \frac{\tau M_c}{\tilde{t}_c}\right)^2}{\left[\left(1 + \frac{M_a}{\tilde{t}_a^2} + \frac{M_b}{\tilde{t}_b^2} + \frac{1}{\tilde{t}_h}\right) - \left(\tau - \frac{\tau M_c}{\tilde{t}_c}\right)\right]\tilde{t}_{\rm cyc}}, \tag{15}$$

respectively, with $\tilde{t}_{\rm cyc} = \tilde{t}_a + \tilde{t}_b + \tilde{t}_c + \tilde{t}_h$. The dimensionless form of the total entropy production (6) becomes

$$\tilde{\sigma} \equiv \frac{\sigma}{\Delta S} = \frac{M_a}{\tilde{t}_a^2} + \frac{M_b}{\tilde{t}_b^2} + \frac{M_c}{\tilde{t}_c} + \frac{1}{\tilde{t}_h}. \tag{16}$$

To reveal the machine performance under maximal cooling rate, we maximize $\tilde{R}$ by setting $\partial\tilde{R}/\partial\tilde{t}_c = 0$, leading to

$$\frac{\tilde{Q}_c^{\,m\tilde{R}}}{\tilde{t}_{\rm cyc}^{\,m\tilde{R}}} = \frac{\tau}{\tilde{t}_c^{\,m\tilde{R}}}\frac{M_c}{\tilde{t}_c^{\,m\tilde{R}}}. \tag{17}$$

This, together with equation (16), gives rise to

$$\frac{-\tilde{Q}_c^{\,m\tilde{R}}}{\tau\tilde{Q}_h^{\,m\tilde{R}} + \tilde{Q}_c^{\,m\tilde{R}}} = \frac{\frac{M_c}{\tilde{t}_c^{\,m\tilde{R}}}}{\left(\frac{M_a}{(\tilde{t}_a^{\,m\tilde{R}})^2} + \frac{M_b}{(\tilde{t}_b^{\,m\tilde{R}})^2} + \frac{M_c}{\tilde{t}_c^{\,m\tilde{R}}} + \frac{1}{\tilde{t}_h^{\,m\tilde{R}}}\right)\left(\frac{\tilde{t}_c^{\,m\tilde{R}}}{\tilde{t}_{\rm cyc}^{\,m\tilde{R}}}\right)}. \tag{18}$$

It follows, using $\tilde{\varepsilon}^{m\tilde{R}} = -\tilde{Q}_c^{\,m\tilde{R}}/(\tilde{Q}_h^{\,m\tilde{R}} + \tilde{Q}_c^{\,m\tilde{R}})$ and $\tau = \varepsilon_C/(1 + \varepsilon_C)$, that the coefficient of performance at maximum cooling rate takes the form

$$\tilde{\varepsilon}^{m\tilde{R}} = \frac{F_2\varepsilon_C}{F_1 + F_2 + F_1\varepsilon_C}, \tag{19}$$

where use of $F_1 = \tilde{t}_c^{\,m\tilde{R}}/\tilde{t}_{\rm cyc}^{\,m\tilde{R}}$ and $F_2 = \left(\frac{M_c}{\tilde{t}_c^{\,m\tilde{R}}}\right)\Big/\left(\frac{M_a}{(\tilde{t}_a^{\,m\tilde{R}})^2} + \frac{M_b}{(\tilde{t}_b^{\,m\tilde{R}})^2} + \frac{M_c}{\tilde{t}_c^{\,m\tilde{R}}} + \frac{1}{\tilde{t}_h^{\,m\tilde{R}}}\right)$ has been made. Since both F_1 and F_2 are situated between [0, 1], namely, $0 \leqslant F_1 \leqslant 1$ and $0 \leqslant F_2 \leqslant 1$, the upper and lower bounds of the optimal coefficient (19) is recovered [46]: $0 \leqslant \tilde{\varepsilon}^{m\tilde{R}} \leqslant \varepsilon_C/(2 + \varepsilon_C)$.

Another optimization objective we consider is the scaled figure of merit $\tilde{\chi}$, which is defined by $\tilde{\chi} = \tilde{\varepsilon}\tilde{R}$. When maximizing $\tilde{\chi}$ by setting $\partial\tilde{\chi}/\partial\tilde{t}_i = 0$, we have

$$\frac{2M_a\mathcal{Z}}{(\tilde{t}_a^{\,m\tilde{\chi}})^2} = -\frac{1}{\tilde{t}_b^{\,m\tilde{\chi}}\tilde{t}_c^{\,m\tilde{\chi}}\tilde{t}_h^{\,m\tilde{\chi}}}(\tilde{Q}_h^{\,m\tilde{\chi}} + \tilde{Q}_c^{\,m\tilde{\chi}}), \tag{20}$$

$$\frac{2M_b\mathcal{Z}}{(\tilde{t}_b^{\,m\tilde{\chi}})^2} = -\frac{1}{\tilde{t}_a^{\,m\tilde{\chi}}\tilde{t}_c^{\,m\tilde{\chi}}\tilde{t}_h^{\,m\tilde{\chi}}}(\tilde{Q}_h^{\,m\tilde{\chi}} + \tilde{Q}_c^{\,m\tilde{\chi}}), \tag{21}$$

$$\frac{Z}{\tilde{t}_h^{m\tilde{\chi}}} = -\frac{1}{\tilde{t}_a^{m\tilde{\chi}}\tilde{t}_b^{m\tilde{\chi}}\tilde{t}_c^{m\tilde{\chi}}}(\tilde{Q}_h^{m\tilde{\chi}} + \tilde{Q}_c^{m\tilde{\chi}}), \tag{22}$$

$$\frac{\tau M_c \mathcal{Z}}{\tilde{t}_c^{m\tilde{\chi}}} = \frac{1}{\tilde{t}_a^{m\tilde{\chi}}\tilde{t}_b^{m\tilde{\chi}}\tilde{t}_h^{m\tilde{\chi}}}(\tilde{Q}_h^{m\tilde{\chi}} + \tilde{Q}_c^{m\tilde{\chi}}), \tag{23}$$

where $\mathcal{Z} = (1/\tilde{t}_a^{m\tilde{\chi}}\tilde{t}_b^{m\tilde{\chi}}\tilde{t}_c^{m\tilde{\chi}} + 1/\tilde{t}_a^{m\tilde{\chi}}\tilde{t}_b^{m\tilde{\chi}}\tilde{t}_h^{m\tilde{\chi}} + 1/\tilde{t}_a^{m\tilde{\chi}}\tilde{t}_c^{m\tilde{\chi}}\tilde{t}_h^{m\tilde{\chi}} + 1/\tilde{t}_b^{m\tilde{\chi}}\tilde{t}_c^{m\tilde{\chi}}\tilde{t}_h^{m\tilde{\chi}})$, and $Q_h^{m\tilde{\chi}}$ ($Q_c^{m\tilde{\chi}}$) is the heat absorbed by the system along the hot(cold) thermal contact under maximum $\tilde{\chi}$. Dividing equation (23) by equations (20), (21) and (22), respectively, we obtain

$$\frac{2M_a}{(\tilde{t}_a^{m\tilde{\chi}})^2} = -\tau\left(\frac{2\tilde{Q}_h^{m\tilde{\chi}}}{\tilde{Q}_c^{m\tilde{\chi}}} + 1\right)\frac{M_c}{(\tilde{t}_c^{m\tilde{\chi}})^2}, \tag{24}$$

$$\frac{2M_b}{(\tilde{t}_b^{m\tilde{\chi}})^2} = -\tau\left(\frac{2\tilde{Q}_h^{m\tilde{\chi}}}{\tilde{Q}_c^{m\tilde{\chi}}} + 1\right)\frac{M_c}{(\tilde{t}_c^{m\tilde{\chi}})^2}, \tag{25}$$

$$\frac{1}{(\tilde{t}_h^{m\tilde{\chi}})^2} = -\tau\left(\frac{2\tilde{Q}_h^{m\tilde{\chi}}}{\tilde{Q}_c^{m\tilde{\chi}}} + 1\right)\frac{M_c}{(\tilde{t}_c^{m\tilde{\chi}})^2}. \tag{26}$$

From equations (24), (25) and (26), we find that the time durations of the four thermodynamic processes are optimally distributed as

$$\frac{\tilde{t}_a^{m\tilde{\chi}}}{\tilde{t}_h^{m\tilde{\chi}}} = \sqrt{2M_a}, \frac{\tilde{t}_b^{m\tilde{\chi}}}{\tilde{t}_h^{m\tilde{\chi}}} = \sqrt{2M_b}, \frac{\tilde{t}_a^{m\tilde{\chi}}}{\tilde{t}_c^{m\tilde{\chi}}} = \sqrt{\frac{2M_a\tilde{\varepsilon}^{m\tilde{\chi}}}{\tau M_c(2+\tilde{\varepsilon}^{m\tilde{\chi}})}}, \tag{27}$$

where $\varepsilon^{m\tilde{\chi}} = -\tilde{Q}_c^{m\tilde{\chi}}/(\tilde{Q}_h^{m\tilde{\chi}} + \tilde{Q}_c^{m\tilde{\chi}})$ is the coefficient of performance under maximum figure of merit $\tilde{\chi}$. Directly adding both sides of equations (20), (21), (22) and (23), we obtain

$$-(\tilde{Q}_h^{m\tilde{\chi}} + \tilde{Q}_c^{m\tilde{\chi}}) = \frac{2M_a}{(\tilde{t}_a^{m\tilde{\chi}})^2} + \frac{2M_b}{(\tilde{t}_b^{m\tilde{\chi}})^2} + \frac{1}{\tilde{t}_h^{m\tilde{\chi}}} - \frac{\tau M_c}{\tilde{t}_c^{m\tilde{\chi}}}\left(\frac{2\tilde{Q}_h^{m\tilde{\chi}}}{\tilde{Q}_c^{m\tilde{\chi}}} + 1\right). \tag{28}$$

With consideration of equations (16) and (28), we have

$$\frac{\tau(\tilde{Q}_h^{m\tilde{\chi}} + \tilde{Q}_c^{m\tilde{\chi}})}{\tau\tilde{Q}_h^{m\tilde{\chi}} + \tilde{Q}_c^{m\tilde{\chi}}} = \frac{2(\frac{M_a}{(\tilde{t}_a^{m\tilde{\chi}})^2} + \frac{M_b}{(\tilde{t}_b^{m\tilde{\chi}})^2} + \frac{M_c}{\tilde{t}_c^{m\tilde{\chi}}} + \frac{1}{\tilde{t}_h^{m\tilde{\chi}}}) - (\frac{2M_c}{\tilde{t}_c^{m\tilde{\chi}}} + \frac{1}{\tilde{t}_h^{m\tilde{\chi}}}) - \tau\frac{M_c}{\tilde{t}_c^{m\tilde{\chi}}}(\frac{2\tilde{Q}_h^{m\tilde{\chi}}}{\tilde{Q}_c^{m\tilde{\chi}}} + 1)}{\frac{M_a}{(\tilde{t}_a^{m\tilde{\chi}})^2} + \frac{M_b}{(\tilde{t}_b^{m\tilde{\chi}})^2} + \frac{M_c}{\tilde{t}_c^{m\tilde{\chi}}} + \frac{1}{\tilde{t}_h^{m\tilde{\chi}}}}. \tag{29}$$

Substitution of $\tilde{Q}_h^{m\tilde{\chi}}/\tilde{Q}_c^{m\tilde{\chi}} = (1+\varepsilon^{m\tilde{\chi}})/\varepsilon^{m\tilde{\chi}}$ and $\tau = \varepsilon_C/(1+\varepsilon_C)$ into equation (29) yields

$$\tilde{\varepsilon}^{M\tilde{\chi}} = \frac{(1-G_1-2G_2)\varepsilon_C + (1-G_1-G_2)\varepsilon_C^2}{4+2(2+G_2)\varepsilon_C - 2G_1(1+\varepsilon_C)} + \frac{\varepsilon_C\sqrt{1+G_2(\varepsilon_C-2)+\varepsilon_C - G_1(1+\varepsilon_C)^2 + 8G_2(2+G_2)\varepsilon_C - G_1(1+\varepsilon_C)}}{4+2(2+G_2)\varepsilon_C - 2G_1(1+\varepsilon_C)}, \tag{30}$$

where $G_1 = \left(\frac{2M_c}{\tilde{t}_c^{m\tilde{\chi}}} + \frac{1}{\tilde{t}_h^{m\tilde{\chi}}}\right)/\tilde{\sigma}^{m\tilde{\chi}}$, $G_2 = \left(\frac{M_c}{\tilde{t}_c^{m\tilde{\chi}}}\right)/\tilde{\sigma}^{m\tilde{\chi}}$, $\tilde{\sigma}^{m\tilde{\chi}} = \left(\frac{M_a}{(\tilde{t}_a^{m\tilde{\chi}})^2} + \frac{M_b}{(\tilde{t}_b^{m\tilde{\chi}})^2} + \frac{M_c}{\tilde{t}_c^{m\tilde{\chi}}} + \frac{1}{\tilde{t}_h^{m\tilde{\chi}}}\right)$. Since $0 \leqslant G_1 \leqslant 2$ and $0 \leqslant G_1 \leqslant 1$, under maximal figure of merit the coefficient of performance (30) satisfies the relation: $0 \leqslant \tilde{\varepsilon}^{m\tilde{\chi}} \leqslant (\sqrt{9+8\varepsilon_C} - 3)/2$ [15, 17].

4. Stability analysis based on the heat amounts exchanged per cycle

Since the mechanism of heat exchange is not explicitly presented in the irreversible machine, the dynamical evolution of the system will be addressed via associating heat exchanged or dissipated to time durations that are dynamical variables. When working under maximal figure of merit, the refrigerator for given control variables remains in the steady state under which these time durations reach a stable point. To proceed, the scaled time durations $\tilde{t}_i$ ($i = a, b, h, c$) can be re-expressed in terms of the fraction of the total cycle period $\tilde{t}_{\rm cyc}$:

$$\tilde{t}_a = \alpha_a\tilde{t}_{\rm cyc}, \tilde{t}_b = \alpha_b\tilde{t}_{\rm cyc}, \tilde{t}_c = \alpha_c\tilde{t}_{\rm cyc}, \tag{31}$$

which thus indicates that $\tilde{t}_h = \alpha_h\tilde{t}_{\rm cyc} = (1-\alpha_a-\alpha_b-\alpha_c)\tilde{t}_{\rm cyc}$. Under maximum figure of merit, the optimal scaled time durations $\tilde{t}_i^{m\tilde{\chi}}$ can be numerically determined by the set of equations (20)–(23) when M_a, M_b, M_c, and τ are given, yielding the optimal values of $\alpha_i^{m\tilde{\chi}}$.

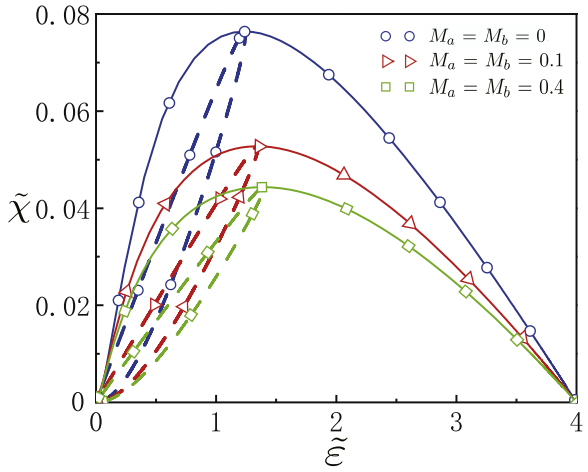

Figure 2. Scaled figure of merit $\tilde{\chi}$ versus scaled coefficient of performance $\tilde{\varepsilon}$ under different constraints. The situation, where $\tilde{t}_{\rm cyc}$ ranges from 0 to ∞ but α_i is set as $\alpha_i = \alpha_i^{m\tilde{\chi}}$, is indicated by the solid parabolic curves, and the case when $\tilde{t}_{\rm cyc}$ is bounded by $\tilde{t}_{\rm cyc}^{m\tilde{\chi}}$ for given $\alpha_i = \alpha_i^{m\tilde{\chi}}$, is denoted by the dashed loop-like curves. The cases correspond to $M_{a,b} = 0$, $M_{a,b} = 0.1$, and $M_{a,b} = 0.4$ are represented in blue lines with circles, red lines with triangles, and green lines with squares, respectively. The other parameters are $M_c = 1$, $\tau = 0.8$.

In figure 2 we plot the figure of merit $\tilde{\chi}$ as a function of coefficient of performance $\tilde{\varepsilon}$ for different models of irreversible refrigeration cycles. In the absence of internal dissipation ($M_{a,b} = 0$), the machine under consideration can reduce to the so-called endoreversible model where the irreversibility is exclusively coming from the thermal interaction between the system and the heat reservoir, and it shows parabolic behavior on the solid curve (with circles). In such a case, the total cycle period $\tilde{t}_{\rm cyc}$ can range from 0 to ∞ while $\alpha_i = \alpha_i^{m\tilde{\chi}}$. We also note that the reversible limit is recovered when and only when $\tilde{t}_{\rm cyc} \to \infty$. However, if $\tilde{t}_{\rm cyc} = \tilde{t}_{\rm cyc}^{m\tilde{\chi}}$ and α_c takes values of 0 to $1 - \alpha_a^{m\tilde{\chi}} - \alpha_b^{m\tilde{\chi}}$, the model where the irreversibility is fixed exists loop-like behavior on the dashed curve (with circles), and it can never reach the reversible limit due its finite time operation.

We consider the model with internal dissipation by adopting $M_{a,b} = 0.1$ and $M_{a,b} = 0.4$, respectively (see also figure 2), using the same approach as in the frictionless case $M_{a,b} = 0$. Like the case in absence of internal friction, the curves (with squares and triangles) for model with friction are also classified into two types of behaviors: parabolic and loop-like. While for the former behavior the cycle period $\tilde{t}_{\rm cyc}$ can take values from 0 to ∞ when $\alpha_{a,b,c} = \alpha_{a,b,c}^{m\tilde{\chi}}$, for the latter $\tilde{t}_{\rm cyc}$ take values from 0 to $\tilde{t}^{m\tilde{\chi}}$. In the reversible case when $\tilde{t}_i \to \infty$, the irreversibility originating from both heat exchange and internal dissipation are all vanishing, and all parabolic curves merges into a point at which $\varepsilon = \varepsilon_C [= \tau/(1-\tau)]$ as they should. When $\tilde{t}_{\rm cyc}$ is bound by $\tilde{t}_{\rm cyc}^{m\tilde{\chi}}$, the irreversibility caused by both heat exchange and friction must exist in such a machine operating in finite time, resulting in loop-like behaviors of curves in figure 2. As emphasized, because of internal dissipation of the working system, an endoreversible model where the adiabatic transformation is frictionless is never realized in finite time, and the additional heat is dissipated into the hot reservoir leading to a decrease in figure of merit $\tilde{\chi}$.

The issue of stability is frequently addressed via a differential equation system. A linear alicization around the stable point allows obtaining the dynamics of a physical quantity q that takes the form: $\mathrm{d}q/\mathrm{d}t = f(q)$ [32–34]. From equations (11) and (12), the dynamics of $\tilde{t}_i$ can be described by an ordinary differential equation system of the form: $\mathrm{d}\tilde{t}_c/\mathrm{d}t = f_c(\tilde{Q}_c(\tilde{t}_c^{m\tilde{\chi}}) - \tilde{Q}_c(\tilde{t}_c))$ and $\mathrm{d}\tilde{t}_j/\mathrm{d}t = f_j(\tilde{Q}_h(\tilde{t}_j^{m\tilde{\chi}}) - \tilde{Q}_h(\tilde{t}_j))$ ($j = a,\ b,\ h$). These f_i ($i = c,\ a,\ b,\ h$) must be monotonically decreasing functions and approach to zero, $f_i = 0$, when $\tilde{t}_i = \tilde{t}_i^{m\tilde{\chi}}$, such that the stationary values of time durations are guaranteed to be stable. We then assume that the dynamic system for $\tilde{t}_i$ can be given by

$$\frac{\mathrm{d}\tilde{t}_c}{\mathrm{d}t} = \kappa_c[\tilde{Q}_c(\tilde{t}_c^{m\tilde{\chi}}) - \tilde{Q}_c(\tilde{t}_c)], \tag{32}$$

$$\frac{\mathrm{d}\tilde{t}_h}{\mathrm{d}t} = \kappa_h[\tilde{Q}_h(\tilde{t}_h^{m\tilde{\chi}}) - \tilde{Q}_h(\tilde{t}_h)], \tag{33}$$

$$\frac{\mathrm{d}\tilde{t}_a}{\mathrm{d}t} = \kappa_a[\tilde{Q}_h(\tilde{t}_a^{m\tilde{\chi}}) - \tilde{Q}_h(\tilde{t}_a)], \tag{34}$$

$$\frac{\mathrm{d}\tilde{t}_b}{\mathrm{d}t} = \kappa_b[\tilde{Q}_h(\tilde{t}_b^{m\tilde{\chi}}) - \tilde{Q}_h(\tilde{t}_b)], \tag{35}$$

where κ_i are respective constants. Here $\tilde{Q}_h$ is the dimensionless amount of heat exchanged along the hot thermal contact under maximal scaled figure of merit $\tilde{\chi}$, and $\tilde{Q}_h(\tilde{t}_j)$ is corresponding amount of heat exchanged as a function of only variable $\tilde{t}_j$ (with $j = a,\ b,\ h$). While $\tilde{Q}_c$ depends only on the time duration t_c, $\tilde{Q}_h$ is dependent not only the time duration t_h but also on time periods $t_{a,b}$. This can be understood by the fact that the entropy generation along two adiabatic strokes increase the amount of entropy variation during the hot thermal contact (cf figure 1 and equation (3)), with this entropy change associated with the corresponding heat exchange (5). The dynamical system has a single steady state when $\tilde{t}_i = \tilde{t}_i^{m\tilde{\chi}}$. In the linear approximation the local stability of this steady state is determined by the eigenvectors and eigenvalues, $\{\lambda_c,\ \lambda_h,\ \lambda_a,\ \lambda_b\}$, of the corresponding Jacobian matrix:

$$\mathcal{J}=-\begin{pmatrix} \kappa_c\frac{\partial\tilde{Q}_c(\tilde{t}_c)}{\partial\tilde{t}_c}\Big|_{(\tilde{t}_c^{m\tilde{\chi}})} & \kappa_c\frac{\partial\tilde{Q}_c(\tilde{t}_c)}{\partial\tilde{t}_h}\Big|_{(\tilde{t}_c^{m\tilde{\chi}})} & \kappa_c\frac{\partial\tilde{Q}_c(\tilde{t}_c)}{\partial\tilde{t}_a}\Big|_{(\tilde{t}_c^{m\tilde{\chi}})} & \kappa_c\frac{\partial\tilde{Q}_c(\tilde{t}_c)}{\partial\tilde{t}_b}\Big|_{(\tilde{t}_c^{m\tilde{\chi}})} \\ \kappa_h\frac{\partial\tilde{Q}_h(\tilde{t}_h)}{\partial\tilde{t}_c}\Big|_{(\tilde{t}_h^{m\tilde{\chi}})} & \kappa_h\frac{\partial\tilde{Q}_h(\tilde{t}_h)}{\partial\tilde{t}_h}\Big|_{(\tilde{t}_h^{m\tilde{\chi}})} & \kappa_h\frac{\partial\tilde{Q}_h(\tilde{t}_h)}{\partial\tilde{t}_a}\Big|_{(\tilde{t}_h^{m\tilde{\chi}})} & \kappa_h\frac{\partial\tilde{Q}_h(\tilde{t}_h)}{\partial\tilde{t}_b}\Big|_{(\tilde{t}_h^{m\tilde{\chi}})} \\ \kappa_a\frac{\partial\tilde{Q}_h(\tilde{t}_a)}{\partial\tilde{t}_c}\Big|_{(\tilde{t}_a^{m\tilde{\chi}})} & \kappa_a\frac{\partial\tilde{Q}_h(\tilde{t}_a)}{\partial\tilde{t}_h}\Big|_{(\tilde{t}_a^{m\tilde{\chi}})} & \kappa_a\frac{\partial\tilde{Q}_h(\tilde{t}_a)}{\partial\tilde{t}_a}\Big|_{(\tilde{t}_a^{m\tilde{\chi}})} & \kappa_a\frac{\partial\tilde{Q}_h(\tilde{t}_a)}{\partial\tilde{t}_b}\Big|_{(\tilde{t}_a^{m\tilde{\chi}})} \\ \kappa_b\frac{\partial\tilde{Q}_h(\tilde{t}_b)}{\partial\tilde{t}_c}\Big|_{(\tilde{t}_b^{m\tilde{\chi}})} & \kappa_b\frac{\partial\tilde{Q}_h(\tilde{t}_b)}{\partial\tilde{t}_h}\Big|_{(\tilde{t}_b^{m\tilde{\chi}})} & \kappa_b\frac{\partial\tilde{Q}_h(\tilde{t}_b)}{\partial\tilde{t}_a}\Big|_{(\tilde{t}_b^{m\tilde{\chi}})} & \kappa_b\frac{\partial\tilde{Q}_h(\tilde{t}_b)}{\partial\tilde{t}_b}\Big|_{(\tilde{t}_b^{m\tilde{\chi}})} \end{pmatrix}. \tag{36}$$

These eigenvalues, which are related to relaxation times $\tilde{t}_i^{\rm re}=-1/\lambda_i$, are easily obtained as $\{\lambda_c,\lambda_h,\lambda_a,\lambda_b\}=\left\{-\kappa_c\frac{\tau M_c}{(\tilde{t}_c^{m\tilde{\chi}})^2},-\kappa_h\frac{1}{(\tilde{t}_h^{m\tilde{\chi}})^2},-\kappa_a\frac{M_a}{(\tilde{t}_a^{m\tilde{\chi}})^3},-\kappa_b\frac{M_b}{(\tilde{t}_b^{m\tilde{\chi}})^3}\right\}$, which are real and negative, and thus the steady state is stable. The operation time can be compared with the total relaxation time, defined by $\tilde{t}_{\rm cyc}^{\rm re}=\tilde{t}_c^{\rm re}+\tilde{t}_h^{\rm re}+\tilde{t}_a^{\rm re}+\tilde{t}_b^{\rm re}$, $\tilde{t}_{\rm cyc}^{m\tilde{\chi}}=\tilde{t}_c^{m\tilde{\chi}}+\tilde{t}_h^{m\tilde{\chi}}+\tilde{t}_a^{m\tilde{\chi}}+\tilde{t}_b^{m\tilde{\chi}}$. Since for the cyclic machine the system should return to the steady state within a cycle period, the total relaxation time should be bounded by total optimal operation time, namely, $\tilde{t}_{\rm cyc}^{\rm re}\leqslant\tilde{t}_{\rm cyc}^{m\tilde{\chi}}$, which constraints κ_i to

$$\frac{(\tilde{t}_c^{m\tilde{\chi}})^2}{\kappa_c\tau M_c}+\frac{(\tilde{t}_h^{m\tilde{\chi}})^2}{\kappa_h}+\frac{(\tilde{t}_a^{m\tilde{\chi}})^3}{\kappa_a M_a}+\frac{(\tilde{t}_a^{m\tilde{\chi}})^3}{\kappa_b M_b}\leqslant\tilde{t}_{\rm cyc}^{m\tilde{\chi}}. \tag{37}$$

Beyond the linear approximation, the system dynamics can be analyzed by numerically solving equations (32), (33), (34), and (35). The velocity vector field of the system can be seen in the three-dimensional stream and the three-dimensional quiver plot on the phase space in figures 3(a) and (b), showing that a stable point exists and its location depends on the internal dissipation coefficient.

The dynamical velocity, $\nu=\sqrt{(\mathrm{d}\tilde{t}_c/\mathrm{d}t)^2+(\mathrm{d}\tilde{t}_h/\mathrm{d}t)^2+(\mathrm{d}\tilde{t}_a/\mathrm{d}t)^2}=$ const, is denoted by the three-dimensional surfaces (see figure 3(a)) that describe patterns over time and indicate how fast the dynamical velocity changes as the system approaches the steady state. The two-dimensional stream plot of dynamics for given time duration $\tilde{t}_{c,h}^{\rm re}$ is shown in figures 4(a) and (b) that results from slicing figure 3(a), comparing with the dynamics without the internal dissipation (see figure 4(c)). The level curves in figures 4(a), (b) and (c) are used to denote constant contours of dynamical velocity, $\nu_0=\sqrt{(\mathrm{d}\tilde{t}_c/\mathrm{d}t)^2+(\mathrm{d}\tilde{t}_h/\mathrm{d}t)^2}=$ const. As internal dissipation decreases, these contours get closer to the stable point and thus the transition to the steady state become faster. The system with smaller dissipation experiences faster transition to the stead state, and the speed of the transition reaches the maximal value when the internal dissipation is vanishing. Hence, the existence of the internal dissipation hinders the process of the system returning to a steady state. Whether the internal dissipation exists or not, the transition to steady state becomes faster when $\tilde{t}_c^{\rm re}<\tilde{t}_c^{m\tilde{\chi}}$ and $\tilde{t}_h^{\rm re}<\tilde{t}_h^{m\tilde{\chi}}$. Near the stable point velocities are slightly slower in the $\tilde{t}_c^{\rm re}$ direction than in the $\tilde{t}_h^{\rm re}$ axis, but as the distances to the stable point increase the transition along $\tilde{t}_c^{\rm re}$ axis becomes much slower. Such a behavior is more symmetric in the ideal adiabatic case.

5. Stability analysis based on the cooling rate and figure of merit

We are now in a position to study the machine performance by optimizing figure of merit χ with respect to the total cycle period and time duration of cold thermal contact. To this end, we introduce the following set of dimensionless variables:

$$L_a=\Sigma_a/\Sigma_T,\ L_b=\Sigma_b/\Sigma_T,\ L_c=\Sigma_c/\Sigma_T,\ L_h=\Sigma_h/\Sigma_T,\ \tilde{t}=\frac{\Delta S}{\Sigma_T}t_{\rm cyc}, \tag{38}$$

where $\Sigma_T=\Sigma_a+\Sigma_b+\Sigma_c+\Sigma_h$ and $t_{\rm cyc}=t_a+t_b+t_c+t_h$. In terms of these variables, the dimensionless heat fluxes, $\dot{\tilde{Q}}_c\equiv\frac{Q_c}{T_c\Delta S\tilde{t}_{\rm cyc}}$ and $\dot{\tilde{Q}}_h\equiv\frac{Q_h}{T_c\Delta S\tilde{t}_{\rm cyc}}$, are given by

$$\dot{\tilde{Q}}_c=\left(1-\frac{L_c}{\alpha_c\tilde{t}_{\rm cyc}}\right)\frac{1}{\tilde{t}_{\rm cyc}}, \tag{39}$$

$$\dot{\tilde{Q}}_h=-\left(1+\frac{L_a}{(\alpha_a\tilde{t}_{\rm cyc})^2}+\frac{L_b}{(\alpha_b\tilde{t}_{\rm cyc})^2}+\frac{L_h}{(1-\alpha_a-\alpha_b-\alpha_c)\tilde{t}_{\rm cyc}}\right)\frac{1}{\tau\tilde{t}_{\rm cyc}}, \tag{40}$$

leading to

$$\tilde{\chi}=\frac{\left[(1-\frac{L_c}{\alpha_c\tilde{t}_{\rm cyc}})\frac{1}{\tilde{t}_{\rm cyc}}\right]^2}{\left(1+\frac{L_a}{(\alpha_a\tilde{t}_{\rm cyc})^2}+\frac{L_b}{(\alpha_b\tilde{t}_{\rm cyc})^2}+\frac{L_h}{(1-\alpha_a-\alpha_b-\alpha_c)\tilde{t}_{\rm cyc}}\right)\frac{1}{\tau\tilde{t}_{\rm cyc}}-\left(1-\frac{L_c}{\alpha_c\tilde{t}_{\rm cyc}}\right)\frac{1}{\tilde{t}_{\rm cyc}}}. \tag{41}$$

It follows that the optimal values of the variables under maximal $\tilde{\chi}$, denoted by $\alpha_a^{m\tilde{\chi}}$, $\alpha_b^{m\tilde{\chi}}$, $\alpha_c^{m\tilde{\chi}}$ and $\tilde{t}_{\rm cyc}^{m\tilde{\chi}}$, can be determined via numerical computation. Following the approach used in the previous section, we have

$$\frac{\mathrm{d}\alpha_c}{\mathrm{d}t}=\mu_c[\dot{\tilde{Q}}_c(\alpha_c^{m\tilde{\chi}},\tilde{t}_{\rm cyc}^{m\tilde{\chi}})-\dot{\tilde{Q}}_c(\alpha_c,\tilde{t}_{\rm cyc})], \tag{42}$$

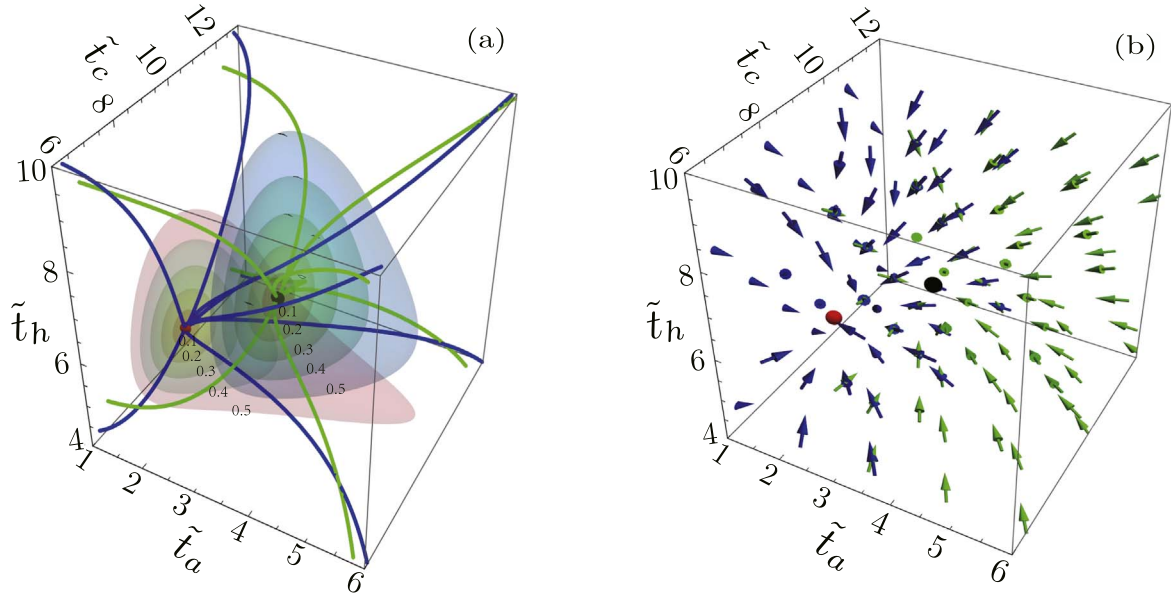

Figure 3. System dynamics determined by equations (32), (33) and (34). Streamline (a) and vector field (b) in plane ($\tilde{t}_a$, $\tilde{t}_c$, $\tilde{t}_h$) are plotted. Three-dimensional surfaces of constant velocities in (a) show how fast the velocity changes as the system relaxes toward the steady state. Green and blue lines (arrows) correspond to the cases $M_a = M_b = 0.4$ and $M_a = M_b = 0.1$, respectively. The other parameters are $\kappa_{a,b,c} = 20$, $\kappa_h = 10$, $M_c = 1$, and $\tau = 0.8$.

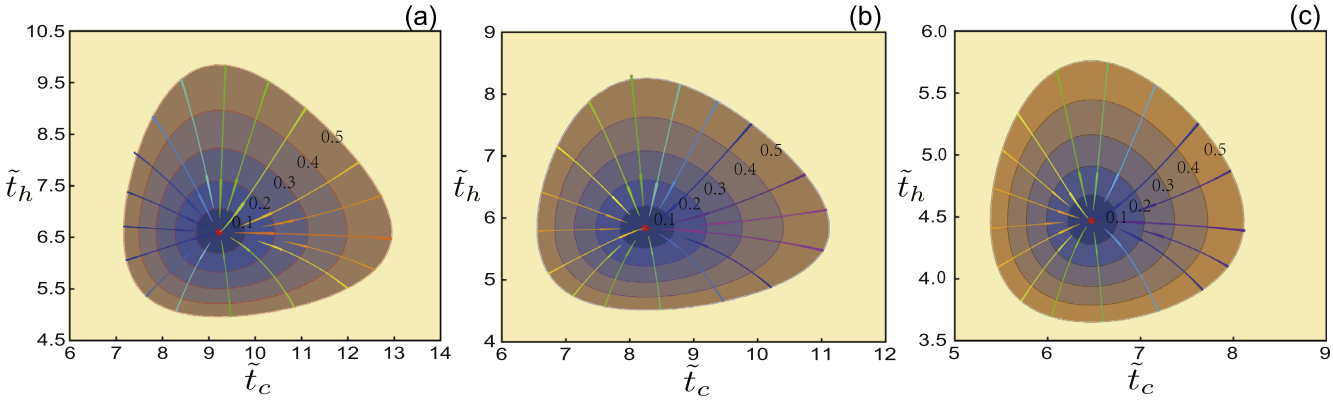

Figure 4. Representative stream plot of the velocity field for (a) $M_{a,b} = 0.4$, (b) $M_{a,b} = 0.1$, and (c) $M_{a,b} = 0$. Dynamical velocity contour indicates the relaxation speed toward the steady states. Level curves of constant velocities show patterns over time and how fast the velocity changes as the system evolves to the steady state. The other parameters are the same as in figure 3.

$$\frac{\mathrm{d}\tilde{t}_{\mathrm{cyc}}}{\mathrm{d}t} = \mu_t[\tilde{\chi}(\alpha_c^{m\tilde{\chi}}, \tilde{t}_{\mathrm{cyc}}^{m\tilde{\chi}}) - \tilde{\chi}(\alpha_c, \tilde{t}_{\mathrm{cyc}})], \tag{43}$$

where $\mu_{c,t}$ are constant. The local stability of the corresponding steady state is determined according to

$$\mathcal{J} = -\begin{pmatrix} \mu_c \dfrac{\partial \dot{\tilde{Q}}_c}{\partial \alpha_c}\Big|_{(\alpha_c^{m\tilde{\chi}}, \tilde{t}_{\mathrm{cyc}}^{m\tilde{\chi}})} & \mu_c \dfrac{\partial \dot{\tilde{Q}}_c}{\partial \tilde{t}}\Big|_{(\alpha_c^{m\tilde{\chi}}, \tilde{t}_{\mathrm{cyc}}^{m\tilde{\chi}})} \\ \mu_t \dfrac{\partial \tilde{\chi}}{\partial \alpha_c}\Big|_{(\alpha_{a,b,c}^{m\tilde{\chi}}, \tilde{t}_{\mathrm{cyc}}^{m\tilde{\chi}})} & \mu_t \dfrac{\partial \tilde{\chi}}{\partial \tilde{t}}\Big|_{(\alpha_{a,b,c}^{m\tilde{\chi}}, \tilde{t}_{\mathrm{cyc}}^{m\tilde{\chi}})} \end{pmatrix}, \tag{44}$$

which becomes after performing the algebra:

$$\mathcal{J} = -\begin{pmatrix} \mu_c \dfrac{\partial \dot{\tilde{Q}}_c}{\partial \alpha_c}\Big|_{(\alpha_c^{m\tilde{\chi}}, \tilde{t}_{\mathrm{cyc}}^{m\tilde{\chi}})} & \mu_c \dfrac{\partial \dot{\tilde{Q}}_c}{\partial \tilde{t}}\Big|_{(\alpha_c^{m\tilde{\chi}}, \tilde{t}_{\mathrm{cyc}}^{m\tilde{\chi}})} \\ 0 & 0 \end{pmatrix}. \tag{45}$$

A null row exists here due to the fact that under maximal figure merit, $\frac{\partial \tilde{\chi}}{\partial \alpha_c}|_{(\alpha_{a,b,c}^{m\tilde{\chi}}, \tilde{t}_{\mathrm{cyc}}^{m\tilde{\chi}})} = \frac{\partial \tilde{\chi}}{\partial \tilde{t}}|_{(\alpha_{a,b,c}^{m\tilde{\chi}}, \tilde{t}_{\mathrm{cyc}}^{m\tilde{\chi}})} = 0$. For this linearized system we thus obtain:

$$\frac{\mathrm{d}\alpha_c}{\mathrm{d}t} = \mu_c \frac{\partial \dot{\tilde{Q}}_c}{\partial \alpha_c}\Big|_{(\alpha_c^{m\tilde{\chi}}, \tilde{t}_{\mathrm{cyc}}^{m\tilde{\chi}})} \alpha_c + \mu_c \frac{\partial \dot{\tilde{Q}}_c}{\partial \tilde{t}}\Big|_{(\alpha_c^{m\tilde{\chi}}, \tilde{t}_{\mathrm{cyc}}^{m\tilde{\chi}})} \tilde{t},$$
$$\mathrm{d}\tilde{t}_{\mathrm{cyc}}/\mathrm{d}t = 0. \tag{46}$$

While $\tilde{t}_{\mathrm{cyc}}$ is constant for any perturbation, the general solution for α_c is of the form $\alpha_c(t) = Ce^{\gamma}$. Since the determinant of $\mathcal{J}$ is zero, one of the eigenvalues is equal to zero, and the other are given by

$$\gamma = \mu_c \frac{\partial \dot{\tilde{Q}}_c}{\partial \alpha_c}\Big|_{(\alpha_c^{m\tilde{\chi}}, \tilde{t}_{\mathrm{cyc}}^{m\tilde{\chi}})}. \tag{47}$$

A relaxation time can be defined by the largest one of the values $\tilde{t}_{\mathrm{re}} = 1/\gamma$. Since the relaxation time must be smaller

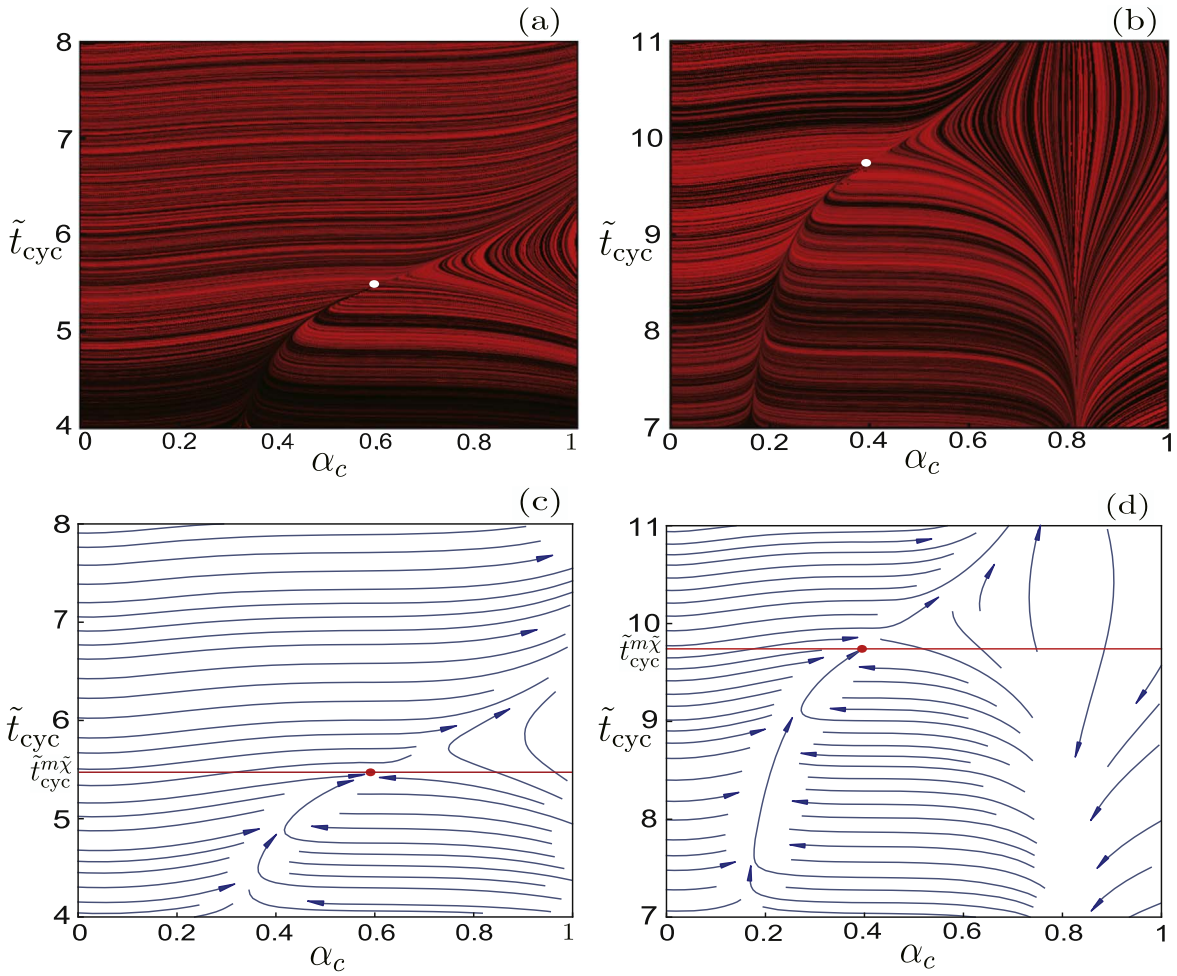

Figure 5. Stability behavior around maximum figure of merit for the system with the dynamics based on equations (42) and (43). The line integral convolution is plotted for (a) $L_{a,b}=0$, $L_{c,h}=0.5$ and (b) $L_{a,b}=0.1$, $L_{c,h}=0.4$. Representative trajectories in phase space are plotted for the system dynamics with (c) $L_{a,b}=0$, $L_{c,h}=0.5$ and (d) $L_{a,b}=0.1$, $L_{c,h}=0.4$. The parameters are $\mu_c=4$, $\mu_t=1$, $\alpha_a=\alpha_a^{m\tilde{\chi}}$, $\alpha_b=\alpha_b^{m\tilde{\chi}}$ and $\tau=0.8$.

than the total cycle time, the possible values of μ should satisfy the constraint: $\tilde{t}_{\rm re}\leqslant\tilde{t}^{m\tilde{\chi}}_{\rm cyc}$.

We are in a position to explore the dynamic behavior of the system under different initial conditions. As an example, we consider the case when the internal dissipation is vanishing. In figure 5 we plot the dynamic behavior linked to the stability near the maximum figure of merit. For given values of μ_t and μ_c, in the first row the line integral convolution is plotted (a) without and (b) with internal dissipation, and in the second row the trajectories in phase space are presented (c) without and (d) with internal dissipation. From figure 5 we observe that, due to internal dissipation, the total cycle time for the machine is increased and the speed of returning to a steady state slows down. The streamlines will pass through the stable point if $\tilde{t}_{\rm re}\leqslant\tilde{t}^{m\tilde{\chi}}_{\rm cyc}$. When $\tilde{t}_{\rm re}>\tilde{t}^{m\tilde{\chi}}_{\rm cyc}$, these streamlines would not be able to spontaneously return to its original operation time, and the machine would stop cycling in this case. The second low in figure 5 shows that the trajectories indicating that the system can reach the steady state are bounded by the irreversible limit (red line) when $\tilde{t}_{\rm re}\leqslant\tilde{t}^{m\tilde{\chi}}_{\rm cyc}$. Physically, fixing the total cycle time would limit the control for the refrigerator and affect the system irreversibility. When imposing constraints over the dynamics of the system, we should make a comparison between the relaxation time and total cycle time in order for the cyclic device to be stable under maximum figure of merit $\tilde{\chi}$.

6. Conclusions

We have investigated the finite-time performance and the local stability for a cyclic refrigerator where the irreversible dissipation originates from both two thermal-contact and two adiabatic strokes. While the irreversible entropy production along the thermal contact satisfies $1/t$-scaling form, the entropy generation during the adiabatic stroke follows the $1/t^2-$ scaling behavior. Under the maximum cooling rate or figure of merit, we recovered the upper and lower bounds of the optimal coefficient obtained in previous models which were, however, limited to the frictionless case.

To discover the dynamical behavior near the maximum figure of merit, we determined a maximum figure of merit by using two approaches: one where the optimization variables are the time durations along four processes, and the other with

optimization variables being the time duration of the cold thermal contact and total cycle period. We took these optimization parameters as dynamic variables governed by restitutive forces. When time durations $\tilde{t}_i$ $(i = a, b, c, h)$ along the four strokes are the dynamic variables, the proposed restitutive forces were assumed to linearly depend on the amount of heat exchanged per cycle. We showed that, like in the refrigerator under maximum Ω function [42], the system can reach the stable steady state at which the figure of merit takes the maximum value, and that relaxation times becomes shorter when $\tilde{t}_c < \tilde{t}_c^{m\tilde{\chi}}$ and $\tilde{t}_h < \tilde{t}_h^{m\tilde{\chi}}$. We found that, when internal friction is involved, the process of system reaching the steady state is hindered, although the stable point exists. On the other hand, when α_c and $\tilde{t}_{\rm cyc}$ are the dynamic variables, we found that the system can approach a locally stable steady-state point under the condition that $\tilde{t}_{\rm re} \leqslant \tilde{t}_{\rm cyc}^{m\tilde{\chi}}$, with $\tilde{t}_{\rm re}$ defined below equation (47). The system will not reach the stable point if $\tilde{t}_{\rm re} > \tilde{t}_{\rm cyc}^{m\tilde{\chi}}$. A similar behavior was also found in the low-dissipation refrigerator under maximal Ω [42]. The value of $\tilde{t}_{\rm cyc}^{m\tilde{\chi}}$ was found to increase as internal dissipation coefficient increases, which means that, when certain conditions are satisfied the transition to the stable state slows down due to the inclusion of internal friction.

Throughout the paper we assumed the dissipation along two adiabatic or two thermal-contact strokes to be symmetric by setting $M_a = M_b$ and $M_c = M_h$, as we only focused on clarifying on the role of inner friction on the stability of machine. The extension of the present analysis to the case when these dissipations are asymmetric could be the next step in order for the role played by the dissipation along each process to be better understood, not only for a refrigerator [42] but also for a heat engine [40, 41]. Another natural extension of our work would be the stability analysis of quantum thermal machines. For quantum systems with inner friction, the time-dependent entropy generation along the thermodynamic adiabatic (but not quantum adiabatic) process can be determined by unitary transformations [34], and a generalization of our calculation to the quantum machines might be an interesting issue for future research. Such a topic would be also useful for understanding the dynamical control on the nonequilibrium quantum systems.

References

[1] Curzon F L and Ahlborn B 1975 *Am. J. Phys.* **43** 22
[2] Andresen B, Salamon P and Berry R S 1984 *Phys Today.* **37** 62
[3] Gordon J M and Huleihil M 1991 *J. Appl. Phys.* **69** 1
[4] Bejan A 1996 *J. Appl. Phys.* **79** 1191
[5] Wang Y and Tu Z C 2013 *Commun. Theor. Phys.* **59** 175
[6] Wu F, Chen L G, Sun F R, Wu C and Li Q 2006 *Phys. Rev.* E **73** 016103
[7] Liu S N and Ou C J 2016 *Entropy* **18** 205
[8] Seifert U 2012 *Rep. Prog. Phys.* **75** 126001
[9] Wu F L, He J Z, Ma Y L and Wang J H 2014 *Phys. Rev.* E **90** 062134
[10] Izumida Y and Okuda K 2008 *Europhys. Lett.* **83** 60003
[11] Ponmurugan M 2020 *Commun. Theor. Phys.* **72** 025601
[12] Schmeidl T and Seifert U 2007 *Europhys. Lett.* **81** 20003
[13] Esposito M, Kawai R, Lindenberg K and Van den Broeck C 2010 *Phys. Rev. Lett.* **105** 150603
[14] Wang J H and He J Z 2012 *Phys. Rev.* E **86** 051112
[15] Hu Y, Wu F F, Ma Y L, He J Z, Wang J H, Hernándezand A C and Roco J M M 2013 *Phys. Rev.* E **88** 062115
[16] Yuan Y, He J Z, Gao Y and Wang J H 2014 *Commun. Theor. Phys.* **61** 344
[17] Wang Y, Li M, Tu Z C, Hernándezand A C and Roco J M M 2012 *Phys. Rev.* E **86** 011127
[18] de Tomás C, Hernándezand A C and Roco J M M 2012 *Phys. Rev.* E **85** 010104(R)
[19] Van den Broeck C 2013 *Europhys. Lett.* **101** 10006
[20] Holubec V and Ryabov A 2015 *Phys. Rev.* E **92** 052125
[21] Sheng S Q, Yang P and Tu Z C 2014 *Commun. Theor. Phys.* **62** 589
[22] Holubec V and Ryabov A 2016 *J. Stat. Mech. J. Stat. Mech.* **7** 073204
[23] Ayala J G, Hernándezand A C and Roco J M M 2017 *Phys. Rev.* E **95** 022131
[24] Johal R S 2017 *Phys. Rev.* E **96** 012151
[25] Ayala J G, Hernándezand A C and Roco J M M 2016 *J. Stat. Mech.* **7** 073202
[26] Sekimoto K and Sasa S 1997 *J. Phys. Soc. Jpn.* **66** 3326
[27] Schmiedl T and Seifert U 2007 *Europhys. Lett.* **81** 20003
[28] Ma Y H, Xu D Z, Dong H and Sun C P 2018 *Phys. Rev.* E **98** 042112
[29] Ma Y H, Xu D Z, Dong H and Sun C P 2018 *Phys. Rev.* E **98** 022133
[30] Bérut A, Arakelyan A, Petrosyan A, Ciliberto S, Dillenschneider R and Lutz E 2012 *Nature* **483** 187
[31] Ma Y H, Zhai R X, Chen J F, Sun C P and Dong H 2020 *Phys. Rev. Lett.* **125** 210601
[32] Liu Q, He J Z, Ma Y L and Wang J H 2019 *Phys. Rev.* E **100** 012105
[33] Chen J C 1994 *J. Phys. D: Appl. Phys.* **27** 1144
[34] Jiao G Q, Xiao Y, He J Z, Ma Y L and Wang J H 2021 *New J. Phys.* **23** 063075
[35] Camati P A, Santos J F G and Serra R M 2019 *Phys. Rev.* A **99** 062103
[36] Feldmann T and Kosloff R 2000 *Phys. Rev.* E **61** 4774
[37] Chen J F, Sun C P and Dong H 2019 *Phys. Rev.* E **100** 062140
[38] Chen J F, Sun C P and Dong H 2019 *Phys. Rev.* E **100** 032144
[39] Ramírez I R, Ayala J G, Hernándezand A C and Santillán M 2017 *Phys. Rev.* E **96** 042128
[40] Ayala J G, Guo J C, Medina A, Roco J M M and Hernándezand A C 2019 *Phys. Rev.* E **100** 062128
[41] Ayala J G, Guo J C, Medina A, Roco J M M and Hernándezand A C 2020 *Phys. Rev. Lett.* **124** 050603
[42] Ayala J G, Medina A, Roco J M M and Hernándezand A C 2020 *Sci. Rep.* **10** 14305
[43] Santillán M, Maya G and Brown F A 2001 *J. Phys. D: Appl. Phys.* **34** 2068
[44] Vargas L G, Ramírez I R and Sánchez N 2005 *J. Phys. D: Appl. Phys.* **38** 1282
[45] Nie W J, He J Z, Yang B and Qian X X 2008 *Appl. Therm. Eng.* **28** 699
[46] Johal R S 2019 *Phys. Rev.* E **100** 052101